

Stirling Solar Engine Design Report



SAN DIEGO STATE UNIVERSITY

Prepared for Professor Kee S. Moon, Ph.D.

Project Advisor Fletcher J. Miller, Ph.D.

Mechanical Engineering 490A

May 18, 2009

Stirling Solar Team Members

*James Baker
Tyler Shaw
Todd Meyer II
Chelsea Tabor*

*619-519-2427
619-208-4325
858-729-4713
858-663-0860*

*jamesbaker@rocketmail.com
shawlawrence@gmail.com
t.k.meyer2gmail.com
Chel.tabor@gmail.com*

INTRODUCTION

Due to rising energy prices and increased interest in renewable energy sources, there has been a large amount of activity in the field of renewable energy sources engineering recently, particularly in the field of solar energy generation. Unfortunately, much of the development of said renewable energy generation has been for utilities, limiting the range of practical applications to large-output arrays, prohibitively expensive technology, and big assemblies which require large parcels of land.

Our design team attempts to remedy the shortcomings of this development trend by designing a residential-scale solar energy generation platform. The performance targets for our system were therefore scaled down to suit the average household's needs in terms of system cost, output power, and space utilization. A current benchmark for small-scale energy generation is \$2 per Watt generated, so we adapted this as a rough target. As a result, we aim to design a very inexpensive solar system which generates between 500 and 1000 Watts, while requiring very little land space.

Currently, the market for residential solar energy systems is dominated by so-called "flat panel" photovoltaic systems. These are identified by their characteristic flat black, rectangular panels and can be seen on rooftops and small parcels of residential land (see Figure 1). The appeal of this technology is their cheap manufacturing cost relative to market alternatives, which will be discussed shortly. However, there are compromises in that flat panel photovoltaic systems have low efficiencies per unit area, forcing customers to cover a large amount of land in order to generate a practical amount of power. At present, such systems are achieving 9-14% efficiency and cost around \$4.30 per Watt.

The technological trend is moving away from these bulky, inefficient panels toward what are called "concentrated" photovoltaics, or CPV. The characteristics of CPV systems are curved mirrors which focus a large amount of sunlight into a small focal point (see Figure 1). Because of the high energy density at the focal point, much smaller photovoltaic cells can be used which get much higher efficiency. In this regard, a CPV system is capable of generating much more power from a smaller area. Currently, CPV systems are approaching 25-40% efficiency, and are approaching a system cost of \$3 per Watt. The disadvantages of CPV systems are higher materials cost due to the more sophisticated high-efficiency PV cells used, as well as the fact that CPV systems must utilize a solar-tracking platform which constantly repositions the mirrored collector in order to maintain an effective focal point. The latter requirement adds a good deal of expense, because of the mechanical complexity and tracking software programming considerations. However, as tracking technology matures, development costs should drop and this issue will be resolved.

While photovoltaic systems are practical for residential applications, the major drawback with the technology is that PV cells are made from exotic semiconductor materials, which add disproportionately to the system cost. In addition, CPV arrays suffer from resistive efficiency losses as panel sizes increase. Due to these considerations, our design team decided to approach the issue from a different angle: the Stirling-cycle engine. This approach has the capability of resolving many of the problems which hold back photovoltaic systems.

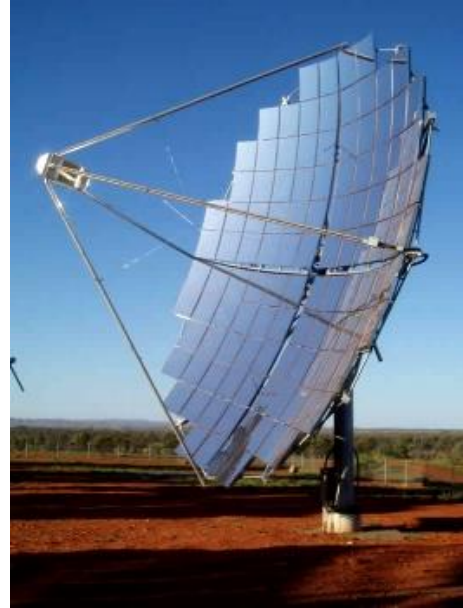


Figure 1: "Flat-panel" PV array and CPV system ^[1, 2]

STIRLING-CYCLE ENGINE BACKGROUND

A Stirling engine creates work from heat energy using the expansion and contraction of a fixed quantity of gas. The expanding gas moves a piston, which in turn generates mechanical work which may be harvested by rotating a crankshaft or employing inducting coils to generate current. One of the benefits of the Stirling engine is that it can create work from practically any heat source. The heat source in the case of our project will be solar radiation, which will be collected and concentrated using a sun-tracking parabolic mirrored dish.

The Stirling engine employs a closed regenerative cycle using a gaseous working fluid (see Figure 2). Essentially, a fixed mass of gas is expanded using a heat source, which displaces a piston (the "power piston"). The gas is then moved into a heat exchanger using a second piston (the "displacement piston") where it cools and contracts. It is then moved by the displacement piston back to the heat source, where the cycle begins again^[3].

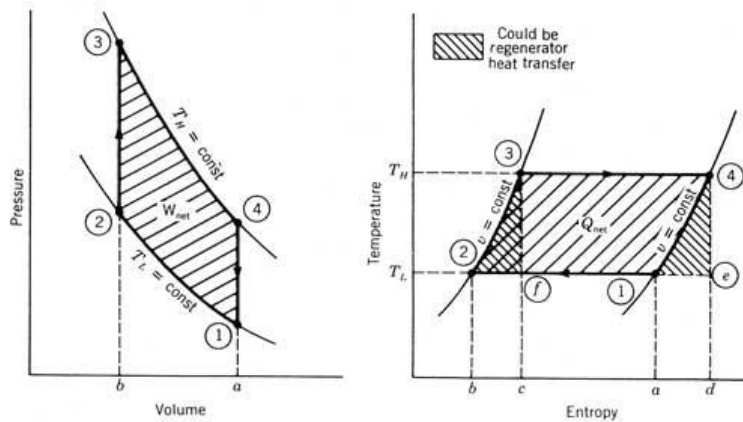


Figure 2: Ideal Pressure-volume and temperature-entropy Stirling cycle diagrams ^[4]

There are many benefits of the Stirling engine design, several of which are evident when compared to photovoltaic (PV) solar power systems of similar scale. The Stirling engine, for example, has a very high efficiency which is theoretically capable of reaching Carnot efficiency (the theoretical thermodynamic limit for energy transfer). Generally, commercial Stirling engines have efficiencies far surpassing standard PV systems, and efficiencies competitive with concentrated photovoltaic (CPV) systems. Because a Stirling engine uses thermal energy to create work, there are no losses due to electrical resistance, as in PV systems. In addition, the engine has few moving parts and requires little maintenance. Finally, Stirling engines utilize inexpensive, readily available materials in their construction, which keep system costs down.

STIRLING ENGINE SYSTEM DESIGN

Stirling engine development on a large scale is extremely complicated, as there are many design factors which must be taken into consideration simultaneously. As can be seen in Figure 3 below from a paper written on Stirling engine design, the process begins with research and specification of important design parameters. In our case, the initial design parameters were desired output, energy input into the system, cost, and working fluid. Then an extensive analysis may be conducted using the well-established Schmidt model for Stirling cycle analysis^[5]. The important engine dimensions can be derived from this model and optimized using advanced thermodynamic analysis. This basic design process of our engine is detailed in the following paragraphs.

Table 1 The Stirling generator design process

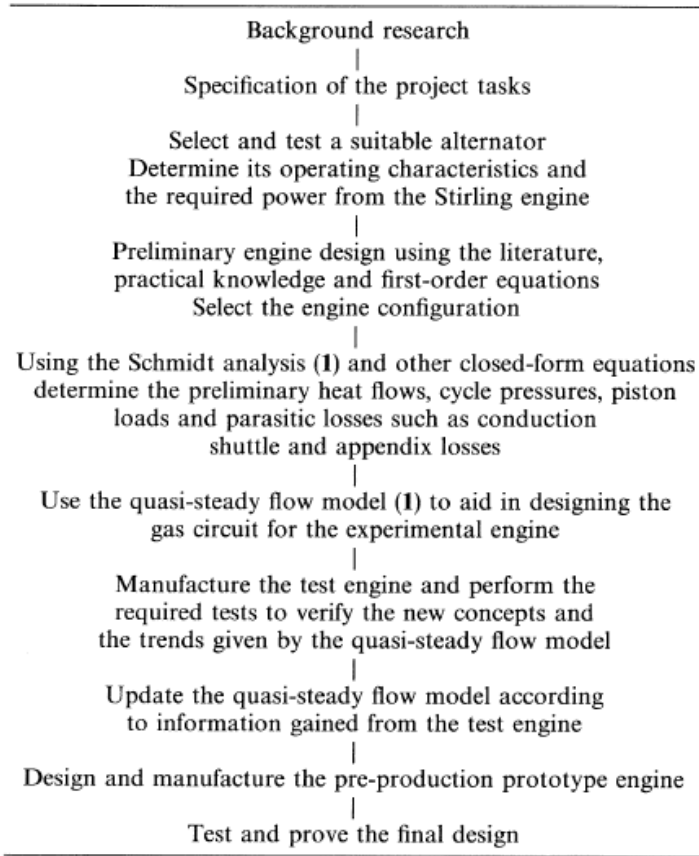


Figure 3: Stirling engine design flow chart ^[7]

- **Solar Concentrator Design**

To begin our design, we first established parameters to guide our efforts. Perhaps the most important factor was that of our energy input into the system, determined mainly by our solar concentrator. We implemented a one square-meter acrylic mirrored parabolic solar concentrator which was donated to us by Dr. Duncan Earl of Sunlight Direct, Inc. (see Figure 4 below).



Figure 4: Our parabolic solar concentrator

This forced us to design to the dishes' particular energy deliver characteristics. It is well established that an approximation for *direct normal* solar irradiance incident on Earth's surface is 1000 Watts per square meter ^[8], although there are more components which effect available solar energy (see Figure 5). Therefore, a perfectly reflecting solar concentrator should be able to deliver this energy into the dishes' focal area.

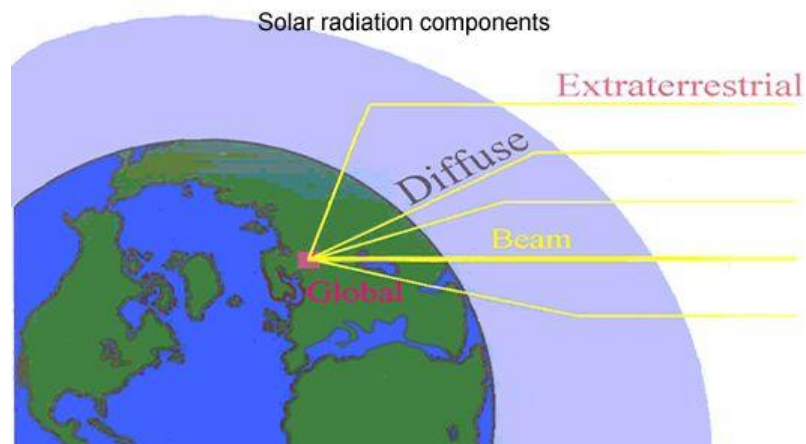


Figure 5: Solar radiation components ^[8]

However, perfect reflectivity is rarely realized, due to imperfections in the mirrored surface and actual physical geometry of the mirror. Therefore, small losses are present in the system, which can reach 10% of incident energy. Based on this initial guess, 900 Watts per square meter of heat flux should have been available to our engine. Empirical testing, however, showed that only a fraction of this energy is transmitted on a typical day^[9]. At this stage, we plan on further refining an experimental setup which will be able to accurately reflect the energy collected from our solar concentrator.

Another design consideration is the packaging of the Stirling engine with respect to the dish. Because placing the Stirling engine at the primary focal point of the concentrator would necessitate a complicated support structure, we chose to locate the engine in the center of the concentrator's hub, and use a secondary mirror placed at the concentrator's focal point in order to re-focus the solar energy onto our engine's energy receiver (see calculations in Appendix A). Acquiring the secondary mirror proved to be a challenge, as high-quality optics are very expensive, and a secondary mirror donated to our team appeared to be ineffective in initial tests, a fault we attribute to the imprecise focus of our segmented concentrator. At this point, we hope to refine the focal point of the segmented concentrator in order to use the high-quality secondary mirror already available to us.

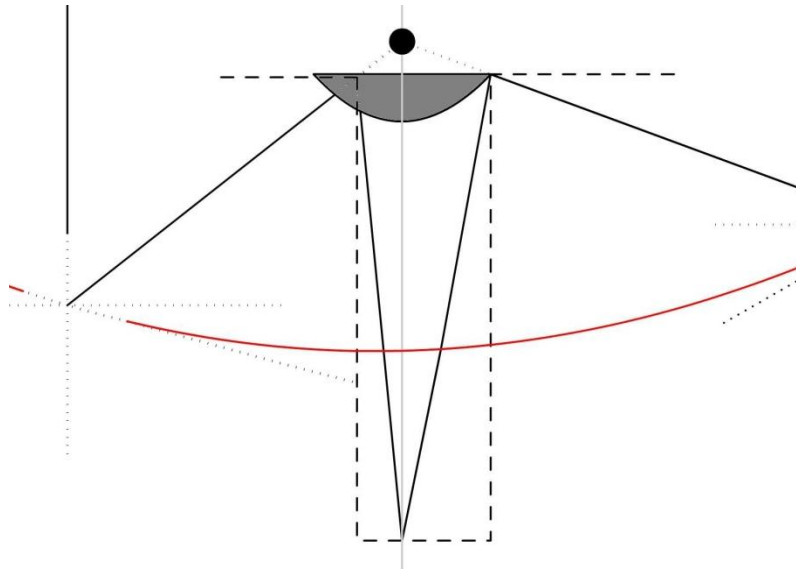


Figure 6: Secondary mirror concept diagram with ray tracing

- **Cost Considerations**

Cost effectiveness was a major theme of our project, and as such, we chose to use inexpensive materials and off-the-shelf components wherever possible in order to reduce our projected production costs. This imposed further design constraints on our design, as we made several critical design decisions based on cost.

First, it was decided that a “beta” type Stirling engine, in which the power and displacement pistons are housed in a common cylinder (see CAD model below), would be much less expensive to machine, and therefore a good choice for our design. It was then agreed that we would avoid expensive machining processes where possible, giving our engine a simple modular format.

Our decision to avoid exotic materials based on the cost considerations guided the design of our solar receiver and regenerator, detailed below. It guided our choice in thermal

receivers from the more expensive pyrolytic graphite to the less expensive nickel oxide. In addition, we were able to choose alumina fiber ceramic blanket as an insulating material because of its low cost. The ceramic blanket is to be inserted in thin strips in between the inner and outer cylinder walls. It was also decided that helium would be our working fluid, as it is inert, allowing us to avoid many of the cost-inflating safety design considerations associated with the ideal hydrogen gas.

- **Pressure Vessel Considerations**

Because the engine is to contain high-pressure Helium gas as its working fluid, considerations had to be taken to prevent failure due to high stresses. This engineering challenge is made more difficult due to the high temperatures the engine operates at. Many materials do not retain high yield strength at the high temperatures we estimate the engine will see (in excess of 500 degrees Celsius). Because of these considerations, we sought a material which would be able to withstand high pressure and temperature loads.

The engine itself is made of three modular cylinders, bolted together with thick flanges typical of high-pressure chambers. Between each segment are insulating carbon-fiber gaskets, which are rated far beyond the pressure and temperature needs of our engine. The two bottom cylinders, which will be seeing the highest temperature loads, were of primary concern to us, and therefore we chose Inconel 600 alloy as the construction material. This nickel alloy is designed for high-temperature use and is commonly implemented in rocket nozzles. As can be seen from Figure 8, Inconel exhibits good yield strength at the operating temperature of our engine.

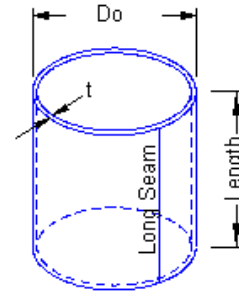
Furthermore, we used a design tool from Pressure Vessel Engineering, which is specifically created for high-pressure pipes. As can be seen below in Figure 7, our engine is of an acceptable thickness for the pressure and temperature we will be seeing. Because safety is another issue when working with pressure vessels, we intend to simulate the final design iteration extensively using computational finite element analysis methods to insure it will survive the engine's working conditions.

6 **Pipe and Shell Design Tool** ver E4.01

7 **Straight Pipe and Shell** Description

8 **Dimensions:**

9	6.000	Do _[in] - outside diameter
10	0.250	t _[in] - nominal wall thickness
11	6.000	L _[in] - length
12	0.010	Corr _[in] - corrosion allowance



13 **Material and Conditions:**

14	Inconel	Material
15	15,000	S _[psi] - allowable stress
16	0.85	EI - long seam efficiency (circ stress)
17	0.70	Ec - circ seam efficiency (long stress)
18	12.5%	UTP [%] - undertolerance allowance
19	500.0	P _[psi] - interior pressure

20 **Calculated Properties:**

21	Volume _[cuft] = ((Do/2-t) ² *pi()*L/1728	((6/2-0.25) ² *Pi()*6/1728 =	0.08
22	Weight _[lb] = (Do-t)*pi()*L*t*40.84/144	(6-0.25)*Pi()*6*0.25*40.84/144 =	7.68

23 **Variables:**

24	UT _[in] = t*UTP	0.25*0.1 =	0.031
25	nt _[in] = t-Corr-UT	0.25-0.01-0.031 =	0.209
26	Ri _[in] = Do/2-nt	6/2-0.209 =	2.791

27 **Required Thickness:** UG-27(c)(1,2)

28	ta _[in] = P*Ri/(S*EI-0.6*P) long seam	500*2.791/(15000*0.85-0.6*500) =	0.112
29	tb _[in] = P*Ri/(2*S*Ec+0.4*P) circ seam	500*2.791/(2*15000*0.7+0.4*500) =	0.066
30	Treq _[in] = MAX(ta,tb)+Corr required minimum thickness	MAX(0.112,0.066)+0.01 =	0.122
31	CheckTreq = Treq <= nt	0.122 <= 0.209 =	Acceptable

32 **Maximum Pressure:** UG-27(c)(1,2)

33	Pint1 _[psi] = (S*EI*nt)/(Ri+0.6*nt)	(15000*0.85*0.209)/(2.791+0.6*0.209) =	913
34	Pint2 _[psi] = (2*S*Ec*nt)/(Ri-0.4*nt)	(2*15000*0.7*0.209)/(2.791-0.4*0.209) =	1619
35	PMax _[psi] = Min(Pint1,Pint2) maximum allowed design pressure	MIN(913,1619) =	912.6
36	CheckP = PMax >= P	912.6 >= 500 =	Acceptable

- 37 Treq provides a worst case required thickness for nozzle analysis for a nozzle located on the long seam or circ seam
- 38 This sheet will not calculate thick walled vessels **Check** → Not a thick walled vessel, calculations are valid
- 39 The UG-16(b) minimum thickness requirement has not been taken into consideration here.
- 40 This sheet cannot be used to check for allowable exterior pressure loads.
- 41 Use the Weld Efficiency program to calculate EI and Ec
- 42 This sheet is for educational use only - use at your own risk.

Figure 7: Pressure vessel calculator initial design results ^[12]

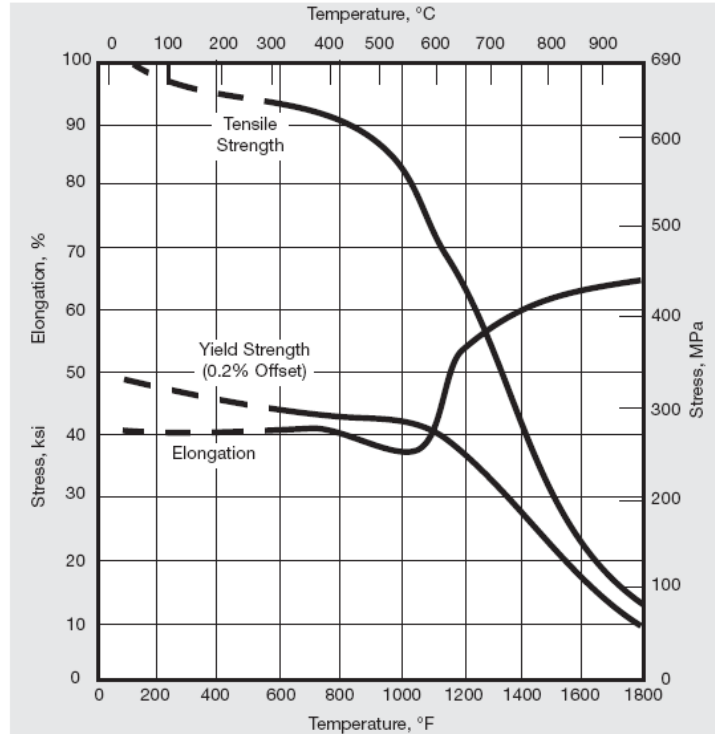


Figure 8: High-temperature tensile properties of annealed, 1600 F/1hr hot-rolled Inconel 600 Plate

- **Solar Receiver Design**

The purpose of the solar receiver is to conduct heat into the working fluid as efficiently as possible, while reducing undesirable heat transfer out of the engine. For this purpose, it was originally considered that a thin, highly conductive piece of pyrolytic graphite could be used as the receiver due to its unique material properties; Disks of pyrolytic graphite are very highly conductive axially, but a thermal insulator radially. Such characteristics would provide high heat conduction to the working fluid, while preventing energy loss through the cylinder head. However, both the high cost and low machinability of graphite had us looking for alternatives.

We then conceived of a transparent head design, consisting of a clear high-temperature material placed over a metallic receiver disk. It was theorized that a transparent head would prevent convective heat transfer from the head, as well as acting as a thermal insulator. A small air gap could also be integrated between the metallic receiver and transparent head, which could theoretically increase the thermal insulation of the receiver disk.

First, in choosing the metallic receiver, we focused on its ability to collect irradiative energy. This quality is based on the absorptivity of a material as well as its emissivity. Certain materials are described as “selective surfaces” because they have high absorptivity but low emissivity. These are desirable for use in solar energy collection, as they retain a large amount of incident radiation. After searching for a material with selective surface qualities, which would also be inexpensive and easy to machine, we decided that nickel III oxide would be ideal for our application. Nickel oxide has a very good absorptivity coefficient of 0.92, with an emissivity of only 0.08^[10]. In addition, nickel is relatively inexpensive and may be machined easily. Nickel III oxide is produced by heating nickel to a high temperature, which oxidizes the metal and turns it dark black, which is an indicator of its high absorptivity. This material is generally sold in metalized powder form, which must be sintered to the desired dimensions. We hope to find the

resources to accomplish this, and examine the sample using an x-ray spectrometer to see if the material is fully oxidized as desired.

For the transparent disk, we selected fused silica, which has a low thermal conductivity (2.17 W/m*K at 800 degrees Kelvin) but retains good optic qualities at high temperatures (see Figure 9). This would be cut into a disk and placed above the metallic receiver, with a small air gap, as mentioned above.

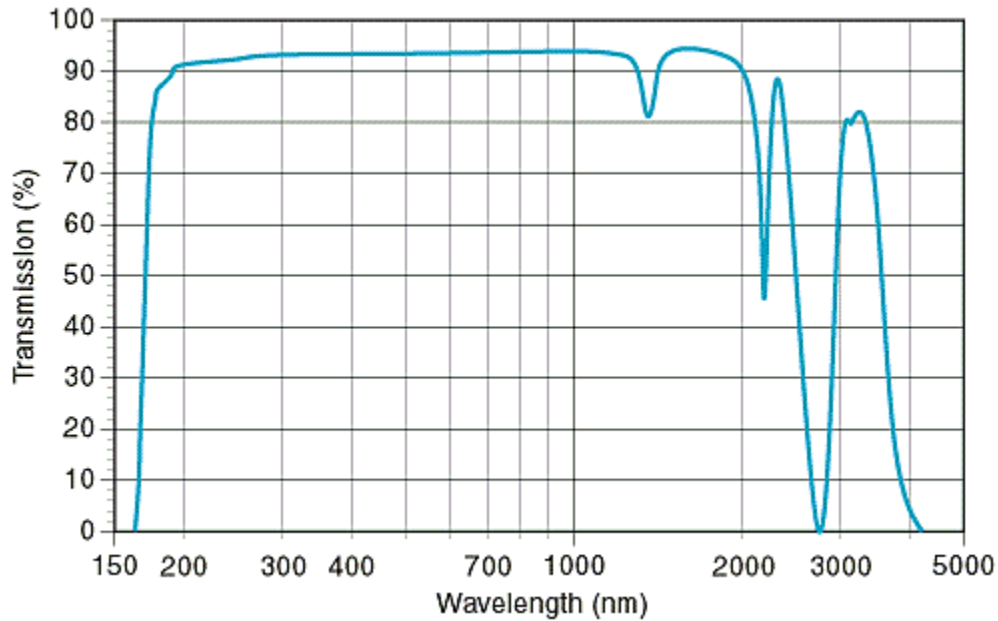


Figure 9: Transmission properties of fused silica ^[11]

- **Engine Internals**

At this point, the engine internals must be iterated further in order to refine the design to an acceptable state. However, rough design parameters have been established in addition to the basic material design considerations.

The engine components will be most likely be made of steel alloy because of its high fatigue life and low cost. In addition, the displacement piston may be constructed from high-temperature Inconel 600 alloy, which maintains a high yield strength at the temperatures the hot side of the engine will be experiencing. The “power” piston, being the only piston which must maintain an atmospheric seal, will be utilizing an “E-type” piston seal (see Figure 10) similar to the TNT-1 Stirling engine^[6] constructed in Japan. It is believed this configuration of piston ring, using Teflon and steel alloy, will allow the greatest pressure seal with the least friction losses.

Beyond these design considerations, the other vital design parameters are the piston diameters and stroke lengths of the piston rods. These dimensions, as stated above, have yet to be refined to an acceptable state, but will be designed in order to produce our desired swept displacement as determined by thermodynamic analysis (see analytical models below). Currently, our swept chamber volume calculations allow a total cylinder volume of roughly 100 cubic centimeters. This is likely to be our final cylinder volume.

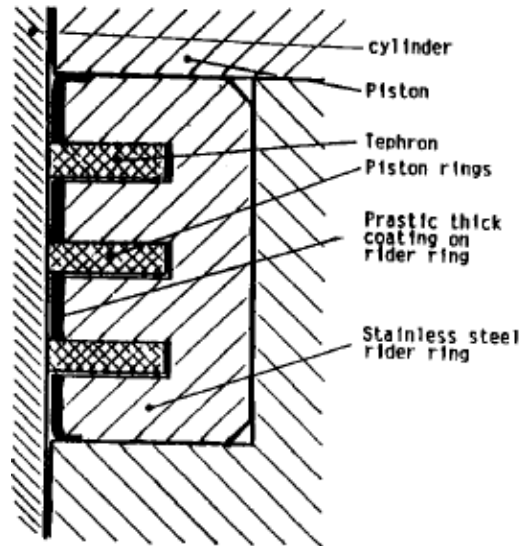


Figure 10: E-Type piston ring schematic ^[6]

- **Drivetrain**

Power delivery had been chosen to be accomplished using camshafts, as opposed to the more traditional linear crankshaft mechanisms. However, the high costs associated with camshaft machining, as well as the extra development time needed for a refined design, caused a design change.

As a result, power delivery was chosen to be accomplished using a crankshaft, connecting rods, and piston rods. The additional connecting rod is used to eliminate off-axis forces, and is kinematically possible by rigidly attaching the piston rods to the pistons. Although there are various power-sapping mechanical losses due to friction present in rod bearings, we have selected the crankshaft because of its proven reliability to transform linear motion to circular motion. In addition to the solution mentioned above, off-axis forces will be reduced further through the addition of two bearings spaced 5 cm apart, along the piston rod. The bearings will be supported by plates welded onto the interior of the mechanical housing cylinder.

The crankshaft will be made from type 304 60% cold rolled steel based on its material properties (1.282 GPa ultimate strength, and 1.027 GPa yield strength). The crankshaft will have three offset crank pins the two outer pins will be in phase and the middle pin will be 90 degrees out of phase with the other two. The two outer crank pins will be offset from the crankshaft axis by 1.5 cm, while the third and middle crank pin will be offset 3 cm; these offsets in combination with the piston cross sectional area define the swept volumes and therefore may change with further iteration. An excel spreadsheet was created to iterate our design, and was based on machine design theory from Robert L. Norton ^{[13][14]}; the result was a crankshaft diameter of 3.2 cm with a safety factor of 2.

- **Regenerator**

The purpose of the regenerator is to act as a thermal capacitor, storing thermal energy in order to increase efficiency of the system by adding and removing thermal energy from the system at key points in the working cycle. A good regenerator should be highly conductive and pass heat to the working fluid as efficiently as possible. Therefore, a ring of copper rods was chosen to accomplish this task. Copper is extremely conductive at high temperatures (398

W/m*K at 225 Celsius), making it an ideal material for this application. In addition, a configuration of tubes oriented co-axially within the cylinder would provide a large surface area for heat convection, while allowing laminar flow of gas along the cylinder axis, aiding advection. We believe this configuration will result in great regenerator efficiencies.

- **Heat Rejecter**

The purpose of the heat rejecter is to remove heat from the working fluid as efficiently as possible. This is critically important, as the theoretical efficiency (also known as Carnot efficiency) of the engine is linearly dependent on the temperature differential between the maximum and minimum temperatures of the engine. The heat rejecter design will likely consist of forced convection-based cooling. In this case, conductive metal fins would be machined onto the upper chassis of the engine so that heat would convect away from the cylinder walls. An inexpensive DC fan could then be implemented to increase airflow and augment cooling. Attempts have been made to model this cooling system using Solidworks' Floworks software, although it proved to be incapable of realistically re-creating the conditions of our engine. We hope to create an accurate model of the engine using Fluent computational fluid dynamics software, and analyze the heat transfer more precisely.

CAD MODEL

At this point, the Solidworks model (see Figure 11 below) represents all major systems and the overall design choices quite well. It displays the essential working functions of the engine and a functioning synthesis of all planned components. However, it is not a complete functioning model. In order to refine the design, we intend to complete a rigorous computational model of the engine's operating conditions, in order to better design the materials to optimize the engine's temperature differential and increase efficiency. Because of this, the CAD model in its current state should be taken as representative of design choices, but not as that of our final design.

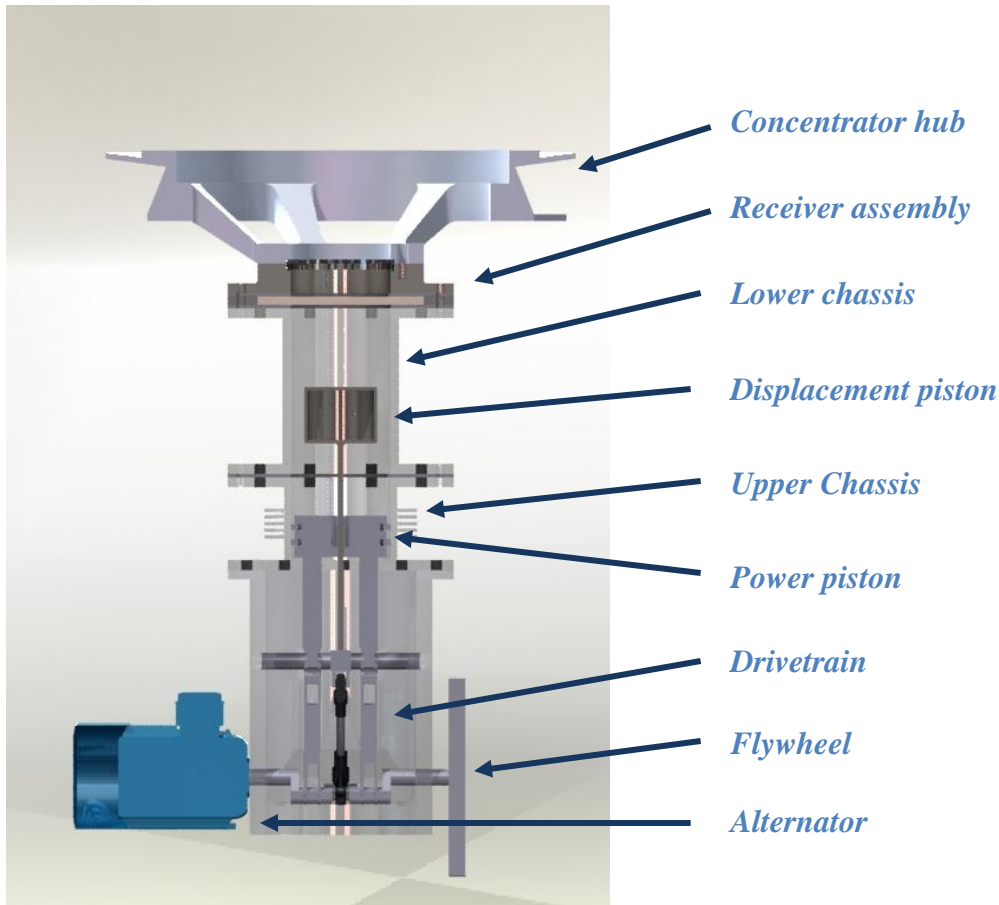


Figure 11: Solidworks concept render

ANALYTICAL MODELS

As the basis of our analysis, we used basic thermodynamic principles and a well-known model known as the Schmidt model. The Schmidt model using the ideal gas law, as well as the sinusoidal variation of the engine volume, in order to compute a theoretical work. Although it is useful for basic analysis, the Schmidt model is not robust enough to provide an extremely accurate representation of engine conditions. A very basic overview of the Schmidt model is discussed below, paraphrased from Jan Machacek's paper^[5].

- *Engine work* can be expressed as the integral of pressure with respect to volume:

- Work of expansion cycle

$$W_E = \int P dV_E = \frac{P_{mean} V_{SE} \pi c \cdot \sin a}{1 + \sqrt{1 - c^2}}$$

- Work of compression cycle

$$W_C = \int P dV_C = - \frac{P_{mean} V_{SE} \pi c t \cdot \sin a}{1 + \sqrt{1 - c^2}}$$

- Total work over complete engine cycle

$$W_i = W_e + W_c$$

- Where *volume change* is expressed sinusoidally, with respect to crankshaft rotation:
 - Overlapping volume of power and displacement pistons

$$V_B = \frac{V_{SE} + V_{SC}}{2} - \sqrt{\frac{V_{SE}^2 + V_{SC}^2}{4} - \frac{V_{SE} \cdot V_{SC}}{2} \cdot \cos \phi}$$

- Total effective volume of displacement piston

$$V_E = \frac{V_{SE}}{2} \cdot (1 - \cos x) + V_{DE}$$

- Total effective volume of power piston

$$V_C = \frac{V_{SE}}{2} \cdot (1 + \cos x) + \frac{V_{SC}}{2} \cdot [1 + \cos(x - \phi)] + V_{DC} - V_B$$

- The total effective system volume change is then

$$V = V_C + V_R + V_E$$

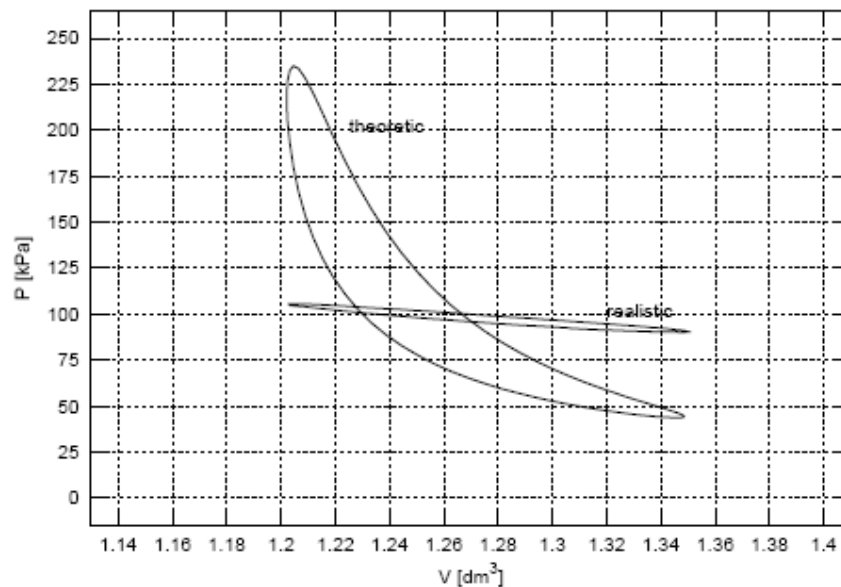


Figure 12: P-V diagrams of realistic and theoretical Stirling engines ^[5]

PLANNED PROGRESS

Over this summer, we first plan on completing a rigorous computational model of the engine using Fluent fluid dynamics software. After attempts were made to model the engine in Solidworks' Floworks application, the software proved inadequate for analyzing the transient states present in Stirling engine operation. After this is completely understood, we plan on conducting another experiment in order to determine the actual heat flux our concentrator is capable of producing, in order to closely match the performance of our engine with that of our dish. Finally, we plan on finalizing all design elements and identifying suppliers for construction materials. We plan on writing all CNC code using Solidworks and Mastercam, in order to do the required machining using SDSU's facilities. We hope to begin bench testing by August 2009.

REFERENCE

- [1] Photo source: Photobucket user "Uoila"; Accessed March 23, 2009;
<http://media.photobucket.com/image/solar%2Bpanels/uoila/solarpanels.jpg>
- [2] Photo source: Vertography.com blog; Accessed March 23, 2009;
<http://blog.vertography.com/wp-content/uploads/2008/08/p8310176.jpg>
- [3] Paraphrased from Wikipedia article, "Stirling engine",
http://en.wikipedia.org/wiki/Stirling_engine
- [4] Photo source: Powerfromthesun.net; Accessed March 23, 2009;
http://www.powerfromthesun.net/chapter12/Chapter12new_files/image022.jpg
- [5] Jan Machacek, "Analysis of Stirling Engine Characteristics by Schmidt's Theory".
Publication date unknown.
- [6] Isshiki, N.; Hashimoto, K.; Watanabe, H.; Shishido, K.; Kikuchi, S.; Watanabe, K. "New Solar Stirling Engine TNT-1 With Direct Internal Radiation Heating" Energy Conversion Engineering Conference, 1989. IECEC-89., Proceedings of the 24th Intersociety. 6-11 Aug 1989 Page(s):2419 - 2424 vol.5
- [7] DM Clucas, JK Raine, "Development of a hermetically sealed Stirling engine battery charger", Department of Mechanical Engineering, University of Canterbury, New Zealand
- [8] "Solar Radiation Basics", University of Oregon Solar Radiation Monitoring Laboratory,
<http://solardat.uoregon.edu/SolarRadiationBasics.html>
- [9] Tyler Shaw, Todd Meyer II, "An Investigation of a Segmented Parabolic Solar Concentrator's Power Output", San Diego State University Dept. of Mechanical Engineering (Early report draft)
- [10] Fundamentals of Heat and Mass Transfer Sixth Edition, Lavine et al, Wiley Press, 2007
- [11] Glass Dynamics LLC data sheet, <http://www.glassdynamicsllc.com/SI-UV%20Material%20Data%20Sheet.htm>
- [12] Pressure Vessel Engineering Pipe and Shell Design Tool,
http://www.pveng.com/m/content/article.php?content_id=294
- [13] Design of Machinery Third Edition, Norton, McGraw Hill, 2004
- [14] Machine Design An Integrated Approach Third Edition, Norton, Prentice Hall, 2006

APPENDIX A – SECONDARY MIRROR CALCULATIONS

Formula for parabolic dish using known coordinates:

$$y = ax^2 + bx$$

$$x, y | 0, 0, 32.5, 11.81, 5.25, 0.30839161$$

$$\begin{bmatrix} 32.5^2 & 32.5 \\ 5.25^2 & 5.25 \end{bmatrix}^{-1} \cdot \begin{bmatrix} 11.81 \\ 0.30839161 \end{bmatrix} = \begin{cases} a \\ b \end{cases}$$

$$a = .0111888$$

$$b = 0$$

$$\boxed{y = .0111888x^2}$$

Secondary Dish calculations:

$$y = .0111888x^2$$

$$\frac{dy}{dx} = 2 \cdot .0111888 x$$

$$\frac{dy}{dx} \bigg|_{32.5} = 2 \cdot .0111888 \cdot 32.5 = .72$$

$$\theta = \tan^{-1} .72 = 36.0273733851^\circ$$

$$\phi = 90 - \theta = 53.9726266149^\circ$$

$$\beta = 180 - 2\phi = 72.0547467702^\circ$$

$$\alpha = 90 - \beta = 17.9452532298^\circ$$

$$x = 8.25852272$$

$$\varphi = 16.8744502534^\circ$$

$$l = 23.0767045$$

$$\lambda = \varphi + \beta = 88.9291970236$$

$$\gamma = \frac{180 - \lambda}{2} = 45.5354014882$$

$$\sigma = \gamma - \alpha = 27.5901482584$$

$$\frac{dy}{dx_{\text{secondary}}} = \tan \sigma = 0.52256844677$$

$$\frac{dy}{dx} = 2ax = 0.52256844677$$

$$a = \frac{0.52256844677}{14} = .037326317626 \approx \frac{1}{27}$$

$$\boxed{y_{\text{secondary}} = \frac{1}{27}x^2}$$